# Indoor Channel Modelling for SISO and Massive SIMO in the 60 GHz mm-Wave Band

Baris Yuksekkaya[1,2]
[1]Department of Electronical and Electronic Engineering, Imperial College London, South Kensington Campus, London, SW7 2AZ, UK
[2]Department of Electronical and Electronic Engineering, Hacettepe University, Beytepe Campus, Ankara, 06800, Turkey
b.yuksekkaya@imperial.ac.uk

***Abstract*—In this paper, an indoor two dimensional channel modeling scheme is proposed for fifth generation (5G) 60 GHz millimeter-wave (mm-wave) communication systems. mm-wave systems are one of the most important candidate technologies to be used in 5G communications because of their advantages such as wide bandwidth, high power communication allowance and small sized, massive numbered antenna arrays. Therefore, modeling of the characteristics of the millimeter-wave channel is substantial.**

**Characterization and modeling studies of mm-wave channels were performed using ray tracing method for both single and massive numbered antennas. The results in terms of multipath delay spread and multipath power content are investigated and a useful simulation is created that will be used to test future hardware implementations.**

***Index Terms*—Wireless communications; mm-wave band; massive SIMO; channel modeling; ray tracing.**

## I. INTRODUCTION

The number of wireless devices accessing wireless networks around the world is increasing rapidly. According to estimates made by Cisco [1], in 2021, mobile devices and connections will reach 11.6 billion and will exceed the world's population. It is also estimated that the worldwide monthly mobile data traffic will exceed 49 Exabits ($49x10^{18}$). This figure is 30 times more than the value measured in 2013. Because of these reasons, new technologies and solutions are needed to provide high data rates under the constraints of Quality of Service (QoS). In particular, bandwidth is an important resource and an important constraint for all wireless systems in this context, since, increased wireless devices will increase the bandwidth used and cause spectrum scarcity. This has necessitated the development of 5G communication systems and the sector has searched for candidate technologies for 5G.

Most of the current wireless services use the frequency range that is below 10 GHz band, which is causing increased intensity. As a result, carrier frequencies in next generation 5G communication systems are expected to move upwards in the spectrum. An obvious indication of this is the unlicensed usage of large bandwidths in the 60 GHz millimeter wave (mm-wave) band. Detailed information on the world-wide rules in this allocated frequency spectrum can be found in [2].

The spectrum range that can be used up to 7 GHz in the 60 GHz band in mm-wave systems is the most important candidate to meet the data rate need in 5G communication systems because of its advantages such as wide bandwidth, high communication power allowance and small size, massive numbered antennas. Therefore, modeling of the characteristics of the millimeter-wave channel is important. Here are a few reasons why the mm-wave range may be attractive:

– The available bandwidth in the mm-wave band is much wider than low frequencies.
– Unlike ultra-wide bands, high power transmission is allowed and more effective isotropic radiated power (EIRP) is available [3], [4].
– It will be subject to lower interference because there are not many applications in this frequency band yet.
– Antenna dimensions will decrease with decreasing wavelength. Thus, a radio frequency (RF) system including antennas and receiver front-end systems will be small in size for mm-wave systems [5].
– Having a small wavelength leads to small antennas which eventually lets using massive number of antennas at the transmitter and/or receiver. This allows having increased array gains and/or antenna diversity gains.

Despite these advantages, the propagation characteristics of mm-wave wireless channels vary widely with respect to low frequency bands. For example, since the free-space path loss at mm-wave frequency is inversely proportional to the carrier frequency, the power losses are much more effective than at low frequencies. Therefore, the communication range is usually short. As a result of these disadvantages, the mm-wave wireless channels must be characterized, modelled and calculated.

The main purpose of this research study is to perform two dimensional (2D) channel modeling operations in order to extract the communication characteristics in the 60 GHz mm-wave band. Ray tracing [6], [7] method is performed in the modeling scheme. Mirror image technique is used in order to find first and higher order reflection paths. The mm-wave channel characteristics in terms of multipath delay

Manuscript received 13 November, 2016; accepted 18 May, 2017.
This research was funded by a grant (No. FBI-2016-9815) from the Scientific Research Department of Hacettepe University.

spread and multipath power content are investigated.

The contributions of the paper can be listed as follows:

– Despite the importance of mm-wave band there is a lack of generic 60 GHz channel models for wireless communications. In order to overcome this situation, comprehensive channel modelling and statistical analysis is performed.

– An understanding of the characteristics of indoor 60 GHz mm-wave band is obtained.

– In addition to generic SISO channels, SIMO channel models with massive number of antennas that are applicable to real-world applications are obtained.

The rest of the paper is as follows. The system model and ray tracing technique is explained in Section II. SISO mm-wave channel modelling and massive SIMO channel modelling procedures and results are given in Sections III and IV, respectively. The discussions and conclusions are given in Section V.

## II. System Model

Consider an indoor room environment that contains a single transmitter (Tx) and a single receiver (Rx) as shown in Fig. 1. For the sake of simplicity, it is assumed that the Tx and Rx are at the same height level and the signal from Tx is only reflected from the side walls, i.e., a 2D channel modelling scheme is performed. This assumption does not alter channel characterization; it is for calculation simplicity and for better understanding the modeling process.

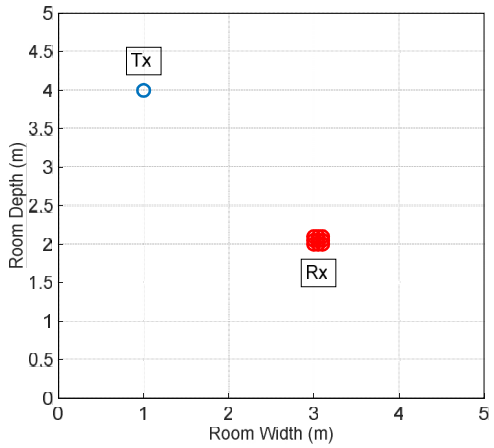


Fig. 1. Indoor channel model.

In the channel modeling process, for the proposed mm-wave system, ray tracing method is performed. In this method, multiple paths to the receiver are obtained. By using multi-path information, a channel impulse response (CIR, $h(t)$) is generated. The mathematical expression of the channel impulse response is given as

$$h(t)=\sum_{k=0}^{K-1}\alpha_k e^{j\varphi_k}\delta(t-\tau_k), \tag{1}$$

where $K$ denotes the number of paths to the receiver, $t$ denotes time index, $\alpha_k$, $\tau_k$, and $\varphi_k$ shows the amplitude, delay, and phase of the $k$th multipath, respectively.

First, the number of antennas in the transmitter and receiver must be decided and the location of the transmitter and receiver must be known. After, the geometry of the possible beams to be directed to the receiving antenna(s) should be examined.

Using the given geometry, after all the multipath distances and reflection angles are found, the channel can be modelled. First, the mm-wave channel amplitude coefficient must be calculated using $\alpha_k=(\rho_k\times o_k\times\gamma_k)^{-1}$, where $\rho_k$, $o_k$, and $\gamma_k$ are the path loss, oxygen absorption, and reflection loss of the $k$th multipath, respectively. Because of indoor modeling, loss caused by rain is ignored.

Path loss is a function depending on frequency and distance and is formulated as

$$\rho_k=\left(\frac{4\pi d_k}{\lambda_c}\right), \tag{2}$$

where $d_k$ is the distance covered by the $k$th path and $\lambda_c$ is the wavelength.

The loss due to oxygen absorption is measured at approximately 15 dB per kilometre [8].

The reflection loss varies depending on the reflecting material and the angle of incidence. Reflective material is accepted as granite in the outdoors and plaster in the indoors. Angle of incidence will be calculated using the geometry and will be selected from a loss table [8], [9].

Afterwards, multiple paths are sorted in descending order and the strongest path takes the index $k=0$. If there is line of sight (LOS), zero index is chosen as LOS. The calculations for delay and phase are performed by taking the strongest path as a reference point. The time delay and the phase of the $k$th path are found as below:

$$\tau_k=\frac{d_k-d_0}{c}, \tag{3}$$

$$\varphi_k=(2\pi F_c\tau_k+\pi N_{r,k})\bmod 2\pi, \tag{4}$$

where $c$ is the speed of light, $F_c$ is the carrier frequency, $N_{r,k}$ is the number of reflections of kth path, and "mod" is the modulus function.

After above operations are performed using scenario geometry, the CIR will be found as the sum of all multiple paths as given in (1).

## III. Ray Tracing and CIR Creation for SISO Channel

### A. Ray Tracing

First, ray tracing procedure for the scenario of a single-antenna transmitter-receiver pair will be examined, and multiple paths will be formed using mirror image method.

The receiver and the transmitter are shown in Fig. 1. The procedure of ray tracing is as follows: First the line of sight (LOS) from Tx to Rx is found, then, first and second order reflection paths are found. The first order (FO) reflection paths are the paths that encounter a single reflection before reaching Tx and the second order (SO) reflection paths are the paths that have two reflections. Higher order reflections

are assumed to be zero because of the increased reflection loss.

Normally, for the given scenario, one would expect to find four FO reflection paths and twelve SO reflection paths (three for each FO reflection path). However, some of these paths are unrealizable paths and these paths should be extracted. A path is unrealizable if the reflected signal path is blocked by an object. This extraction process is also considered in the simulations.

The LOS is a line that is drawn directly from Tx to Rx and shown in Fig. 2.

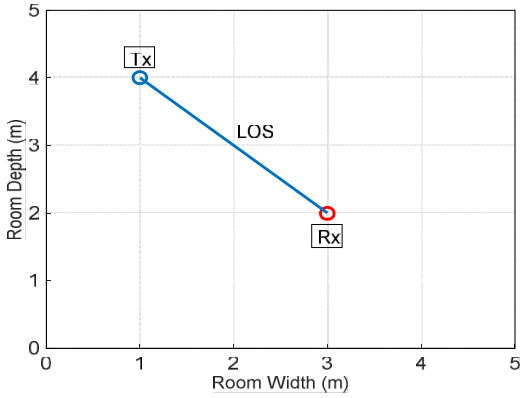


Fig. 2. LOS path for SISO scenario.

Mirror image method is used to find the paths reflecting from the walls. However, it is necessary to put a limit on the paths that will be reflected, or else there will be an infinite number of paths. As shown in the works [10]-[12], the power of the signals that are reflected more than two times experience massive amount of loss and are negligible. For this reason, the signals that usually are used in ray tracing are the FO and SO reflected paths.

In order to find the FO reflection paths, the mirror image of Tx with respect to all of the obstacles (walls) must be created and, considering the images as a source, the paths between these mirror images and Rx should be calculated. The distance between mirror images and Rx give the distance covered by the selected FO reflected paths. This procedure is shown in Fig. 3, where, Tx' is one of the mirror images of Tx (mirror image of Tx with respect to the first wall) and P1 is the point of reflection. Tx'-P1 and Tx-P1 are equidistant, therefore, as discussed, the FO reflection path distances can be calculated using the mirror image coordinates. The reflection angles ($\alpha_{FO,l}$) will be used to calculate the reflection loss, where, $l$ shows the index number of the FO reflection paths.

In order to find the SO reflection paths, the mirror images of FO mirror images should be found as shown in Fig. 4, where, Tx" is one of the SO mirror images of Tx (mirror image of Tx' with respect to the second wall) and P1 and P2 are the first and second reflection points, respectively. The path Tx"-P2 obtained by treating the SO image Tx" as a source is equidistant with the sum of the paths Tx-P1 and P1-P2. Thus, the SO reflection path distances can be calculated using the SO mirror image coordinates. The reflection angles ($\alpha_{SO,l1}$ and $\alpha_{SO,l2}$) will be stored and used to find the reflection loss later.

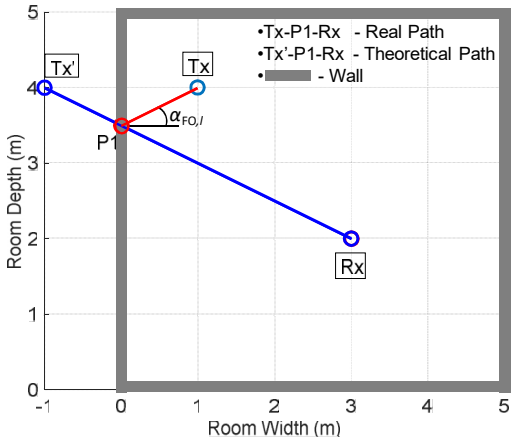


Fig. 3. FO reflection path for SISO scenario.

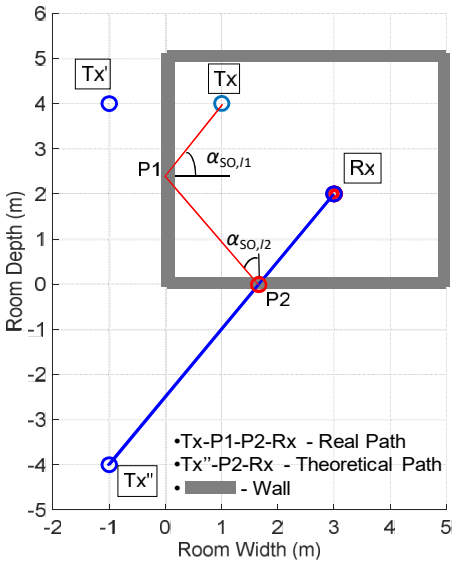


Fig. 4. SO reflection path for SISO scenario.

All multiple paths will be obtained geometrically as shown in Fig. 5, after above procedures are completed for LOS, FO reflection paths, and SO reflection paths. Notice that, there are six second-order reflection paths instead of twelve. This is a result of the extraction of unrealizable paths explained earlier.

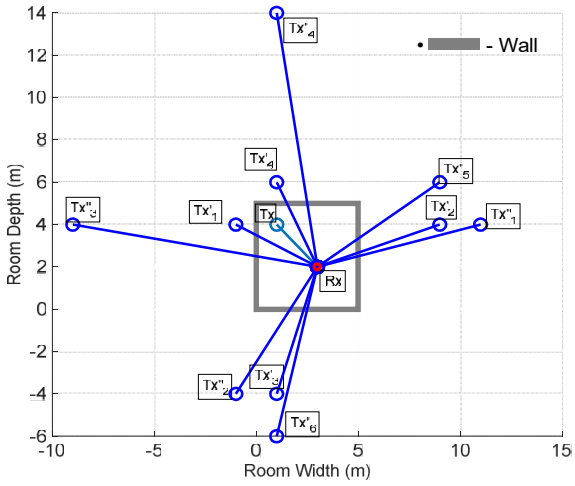


Fig. 5. Multipaths modelled for SISO scenario.

After all multipath distances and reflection angles are found, these properties can be used in the CIR calculating

procedure described in Section II. The channel impulse response will be found as the sum of the multiple paths as shown in (1).

### B. CIR Simulations

In the simulations, the geometry given in Fig. 5 is used, i.e., the room is a 5 m × 5 m square, the Cartesian coordinates of the receiver are taken as (2 m, 3 m) and the coordinates of the transmitter are taken as (1 m, 4 m). Therefore one LOS path, four FO reflection paths and six SO reflection paths are generated. Using the procedure in Section II and (1) the CIR is formed. The normalized amplitude of CIR is given in Fig. 6.

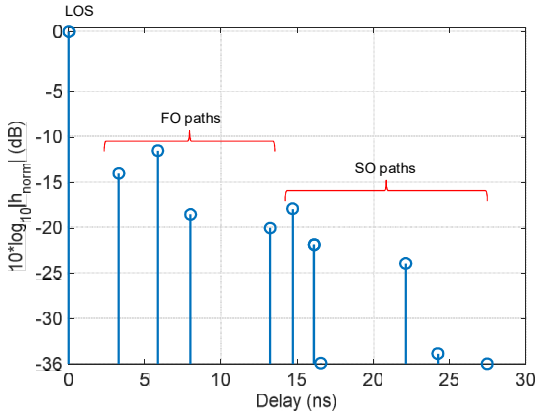


Fig. 6. Amplitude-delay graph of the normalized channel impulse response modelled in the SISO channel scenario.

As seen in Fig. 6, the LOS dominates other multipaths. To investigate the characteristics of the obtained CIR, the power profile of paths and delay spread are investigated.

As shown in Fig. 6, the last multipath delay is in the range 25 ns - 30 ns, which is called the delay spread of the channel. Since the dimensions of the indoor room are 5 m × 5 m, the multipath delay spread cannot increase well above the 25-30ns band for different positions of Tx and Rx, and the approximate delay spread is calculated as 30 ns. Therefore, the coherence bandwidth (inverse of delay spread) becomes 33.3 MHz. It is known that the message signal bandwidth in the 60 GHz band is in the range 1 GHz–2 GHz [8], [9], [13], therefore the scenario examined in this indoor case will be frequency selective [14]. In order to cope with frequency selective channels, equalization or orthogonal frequency division multiplexing (OFDM) methods should be used [14], [15]. Hence, it is also necessary to use technologies like these to cope with frequency selectivity in the proposed mm-wave scenario.

Figure 7 shows the sum power percentage of first 'x' multipaths with respect to full channel power for increasing 'x'. It can be seen in the graph that, 80 % of the total power is in the LOS path and it is also seen that the first 5 multipaths have 99 % of total power. This result shows that, the power information of the channel is stored in the LOS and FO reflection paths. The second-order reflections are weaker relative to LOS and FO reflection paths; however they are still useful in order to model the delay spread.

This concludes the modelling of SISO channel in the mm-wave band. It is expected that the findings presented should be applicable to real-world applications in future works.

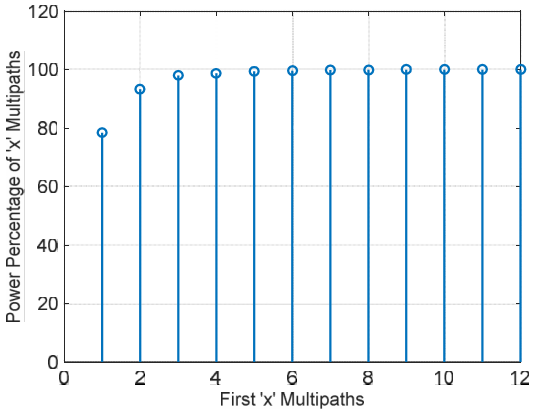


Fig. 7. Power percentage of the first 'x' multipaths in the channel modelled for SISO channel scenario.

## IV. Ray Tracing and CIR Creation for Massive SIMO Channel

### A. Ray Tracing

As mentioned earlier, the loss in the mm-wave band will increase due to the high frequency, e.g., the path loss is inversely proportional to the square of the carrier frequency. However, higher frequency also means smaller wavelength and smaller wavelength will lead to the use of small-sized antennas and decreased distance between antennas. For example, in the 60 GHz band, the wavelength is 5 mm, so the distance between antennas is acceptable as low as 2.5 mm. This will allow a 10 × 10 antenna array to be formed in a 2.5 cm × 2.5 cm area. Thus, 100 antennas will be squeezed into an area of 6.25 $cm^2$, and as a result of 100 antennas the antenna diversity on the performance will be examined.

The receiver and the transmitter were previously shown in Fig. 1. In the receiver with massive antennas scenario, it is assumed that the antennas are in a square array. In the same way as the SISO scenario, first the LOS from Tx to Rx is found, then, FO and SO reflection paths are found. The procedure of generating the geometry of multipaths for each antenna is same as the procedure for SISO scenario. The LOS is a line that is drawn directly from Tx to each antenna of Rx as shown in Fig. 8.

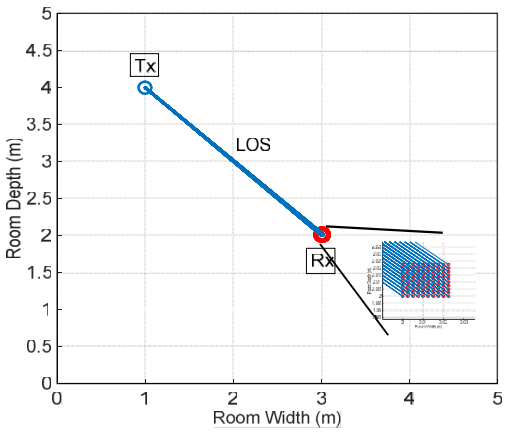


Fig. 8. LOS paths for massive SIMO scenario. The 10 x 10 receive antenna matrix is also shown enlarged.

Mirror image of Tx with respect to four walls are created in order to find the FO reflection paths. The distance

between mirror images and each Rx antenna gives the distances covered by each FO reflected path. This procedure is shown in Fig. 9, where, Tx' is the mirror image at hand and P1 is the point of reflection. The reflection angles will be used to calculate the reflection loss.

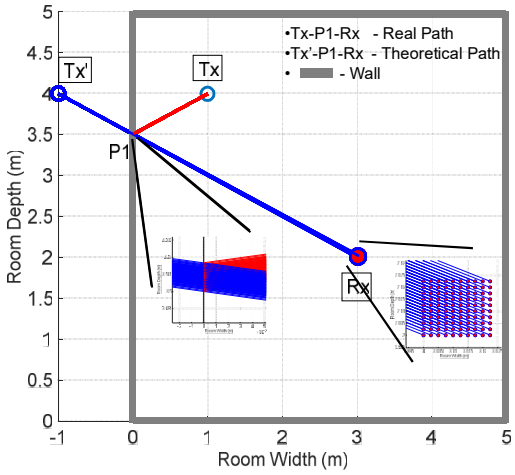


Fig. 9. FO reflection paths for massive SIMO scenario. The reflection points and antenna array are enlarged.

As in the SISO scenario, the mirror images of FO mirror images are used to find the SO reflection paths as shown in Fig. 10. Here, Tx" is one of the SO mirror images and P1 and P2 are the first and second reflection points, respectively. The distance between SO mirror images and each Rx antenna gives the distances covered by each SO reflected path. The reflection angles will be stored and used to find the reflection loss later.

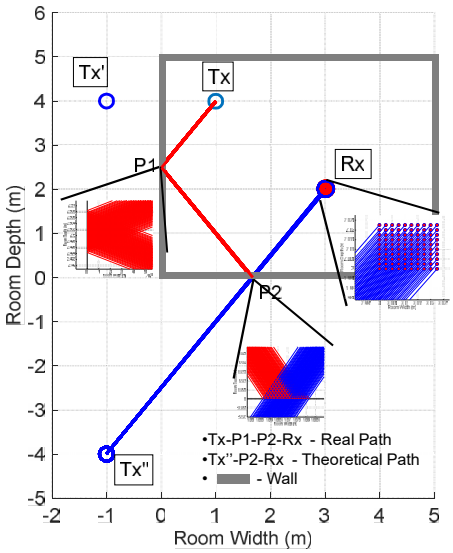


Fig. 10. SO reflection paths for massive SIMO scenario. The reflection points and antenna array are enlarged.

After the ray tracing procedures are achieved for LOS, FO reflection paths, and SO reflection paths of all antennas, all of the multiple paths will be obtained geometrically as shown in Fig. 11.

Again, after the geometry formation procedure is accomplished, the multipath distances, reflection angles, and mm-wave channel characteristics can be used in the CIR calculating procedure described in Section II. Again, the CIR is found using (1).

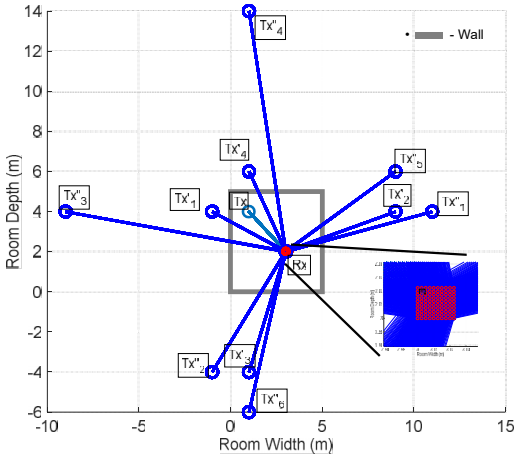


Fig. 11. Multiple paths in the channel modelled for the SIMO channel scenario. The 10 × 10 receive antenna matrix is also shown enlarged.

## B. CIR Simulations

For the computer simulations, the geometry given in Fig. 11 is used, where the room is the same room in the SISO scenario, the coordinates of the transmitter are taken as (1 m, 4 m), and the first element of the receiver antenna array is placed at (2 m, 3 m). The antenna array is a 10 × 10 square array (100 antennas) and antenna spacing is chosen as half wavelength, i.e., 2.5 mm for 60 GHz communication. Therefore, for the given geometry, there are 100 LOS paths, 400 FO reflection paths and 600 SO reflection paths from Tx to the Rx antenna array. Using the procedure in Section II and in (1) CIR is formed as a channel matrix (combination of 11 multipath vectors sized 100 × 1).

It is expected that the channels of each antenna should have a similar CIR to that of the SISO CIR since the antenna spacing is distant enough for each channel to have independent fading characteristics. The results are as anticipated. The normalized amplitude of the CIR of one antenna is given in Fig. 12. As in the SISO case, the LOS impulse dominates other multipath impulses. Moreover the delay spread is also similar to the SISO scenario range of 30 ns–35 ns which indicates a frequency selective channel scenario.

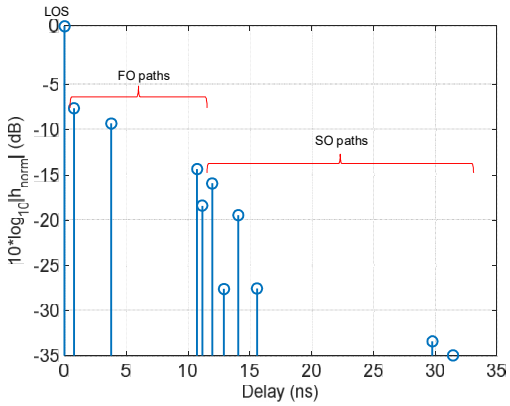


Fig. 12. Amplitude-delay graph of the normalized channel impulse response of one antenna in the massive SIMO channel scenario.

Again, it is impossible to show the results for each antenna, hence, Fig. 13 shows the sum power percentage of first 'x' multipaths of one antenna. It is seen that 99 % of total power is concentrated in the first 5 multipaths. Thus SO

reflection paths are weaker than LOS and FO reflection paths.

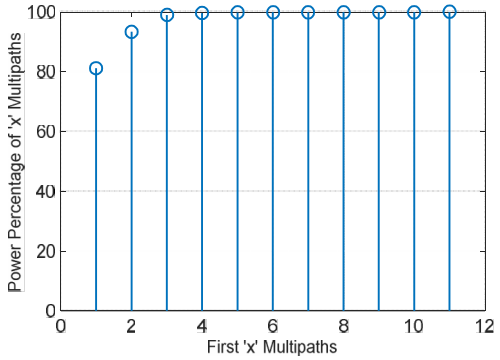


Fig. 13. Power percentage of the first 'x' multipaths in one antenna channel for massive SIMO channel scenario.

As discussed earlier, as a result of massive number of receive antennas two types of performance increase occur, one of them is array gain and the other is receive antenna diversity. The array gain occurs when receive signals are combined coherently, and array gain will be available even if there is no fading. The other performance gain is receive antenna diversity, which is a result of combining independent fading paths. The combining for both scenarios can be done in several ways such as selection combining, threshold combining, and maximal ratio combining [14]. As an example perfect combination of the 100 antennas in the given example is given in Fig. 14.

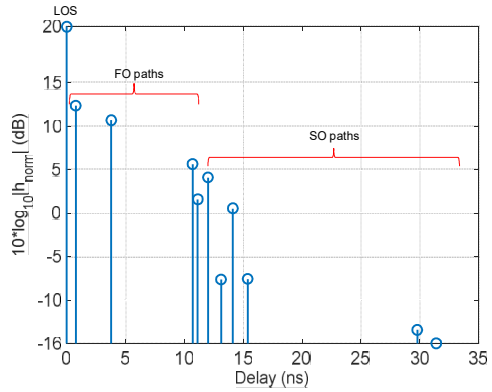


Fig. 14. Amplitude-delay graph of the channel impulse response for perfect combination in the massive SIMO channel scenario.

The perfect combination in Fig. 14 is unrealizable in real life, however, it can give some insight and an upper bound on the array gains and antenna diversity gains in mm-wave band.

Thus, the advantages and disadvantages of the obtained mm-wave compatible channels have been demonstrated.

## V. CONCLUSIONS

This paper tries to inspire an understanding of the characteristics of indoor 60 GHz mm-wave band for single antenna and massive antenna systems. It is also aimed to overcome lack of generic 60 GHz channel models for SISO and massive SIMO that are applicable to real-world applications in the literature.

The channel models were created using ray tracing method with mirror image technique. Channel impulse responses are constructed and examined in terms of power content and multipath delay spread. The length of delay spread showed that the indoor channel is frequency selective and as a future work OFDM-based mm-wave receivers should be developed. Moreover, simulations showed the dominance of LOS path and also it showed that 99 % of power is contained in the LOS and FO reflection paths.

In the massive SIMO case, it is also seen that 100 antennas take up just 6.25 $cm^2$ space and all of these massive numbered antennas can be used to achieve increased array gain and receive antenna diversity gain.

## REFERENCES

[1] *Cisco Visual Networking Index: Global Mobile Data Traffic Forecast Update, 2016-2021*, Cisco, 2017

[2] S. K. Yong, C.-C. Chong, "An overview of multigigabit wireless through millimeter wave technology: Potentials and technical challenges", *EURASIP J. Wireless Commun. and Networking,* 2007. [Online]. Available: http://dx.doi.org/10.1155/2007/78907

[3] *Millimeter-Wave Propagation: Spectrum Management Implications*, Federal Communications Commission Document, 1997.

[4] T. S. Rappaport, R. W. Heath Jr., R. C. Daniels, J. N. Murdock, *Millimeter Wave Wireless Communications*. Upper Saddle River, NJ: Pearson Education, 2014.

[5] M. S. Alam, M. T. Islam, N. Misran, "Inverse triangular shape CPWfed antenna loaded with EBG reflector", *Electronics Letters,* vol. 49, no. 2, pp. 86–88, 2013. [Online]. Available: http://dx.doi.org/ 10.1049/ el.2012.3957

[6] ] S. Kubal, M. Kowal, P. Piotrowski, R. J. Zielinski, "Radiation characteristics of simple irregular surface", in *Int. Symposium on Electromagnetic Compatibility,* 2012, pp. 1–5. [Online]. Available: http://dx.doi.org/10.1109/EMCEurope.2012.6396684

[7] L. Der-Song, "6F-5 Characterization of Fabrication Related GapHeight Variations in Capacitive Micromachined Ultrasonic Transducers", in *Proc. of the IEEE Ultrasonics Symposium,* 2007, pp. 523–526.

[8] M. K. Samimi, T. S. Rappaport, "Characterization of the 28 GHz millimeter-wave dense urban channel for future 5G mobile cellular", *NYU Wireless Technical Report 1,* 2014.

[9] T. S. Rappaport, *et al*., "Millimeter wave mobile communications for 5G cellular: It will work!", *IEEE Access,* vol. 1, pp. 335–349, 2013. [Online]. Available: http://dx.doi.org/10.1109/ACCESS.2013. 2260813

[10] R., Wonil, *et al*., "Millimeter-wave beamforming as an enabling technology for 5G cellular communications: Theoretical feasibility and prototype results", *IEEE Communications Magazine*, vol. 52, pp. 106–113, 2014. [Online]. Available: http://dx.doi.org/10.1109/ MCOM.2014.6736750

[11] S. Hur, *et al*., "Proposal on millimeter-wave channel modeling for 5G cellular system", *IEEE J. of Selected Topics in Signal Processing*, vol. 10, pp. 454–469, 2016. [Online]. Available: http://dx.doi.org/ 10.1109/JSTSP.2016.2527364

[12] S. A. Iyanda, *et al*., "Radio propagation path loss models for 5G cellular networks in the 28 GHz and 38 GHz millimeter-wave bands", *IEEE Commun. Magazine*, vol. 52, pp. 78–86, 2014. [Online]. Available: http://dx.doi.org/10.1109/MCOM.2014.6894456

[13] E. Torkildson, M. Upamanyu, M. Rodwell, "Indoor millimeter wave MIMO: Feasibility and performance", *IEEE Trans. Wireless Commun.*, vol. 10, pp. 4150–4160, 2011. [Online]. Available: http://dx.doi.org/10.1109/TWC.2011.092911.101843

[14] A. Goldsmith, *Wireless Communications*. Cambridge, UK: Cambridge University Press, 2005. [Online]. Available: http://dx.doi.org/10.1017/CBO9780511841224

[15] R. V. Nee, P. Ramjee, *OFDM for Wireless Multimedia Communications*. Norwood, MA: Artech House, Inc., 2000.